A monolithic micro-tensile tester fabricated by femtosecond laser to investigate fused silica mechanical properties

Christos-Edward Athanasiou[a] and Yves Bellouard

Galatea lab, STI/IMT, Ecole Polytechnique Fédérale de Lausanne (EPFL)
Rue de la Maladière, 71b, CH-2002 Neuchâtel, Switzerland

Abstract. We present an experimental method to fill in the existing gap of characterization tools for the mechanical testing of fused silica and silica's polymorphic phases in the micro- and nano- scales. The approach is based on a monolithic tensile tester, entirely made of fused silica for which the same femtosecond laser in not only used for the fabrication of the device, but also for its operation (loading the specimen) as well as for *in situ* measuring deformations resulting from the test beam's elongation, thanks to the use of the third harmonic generation (THG). The use of the THG as an in-line laser metrology tool is extensively discussed. The validity of the experimental approach is presented by the direct elastic modulus measurement of fused silica at high stresses up to 1.8 GPa.

1 Introduction

SiO_2 [1] is one of the most studied materials not only due to its practical importance in various technological fields such as optics, electronics and chemistry, but also due to its importance in geosciences [3]. Fused silica – the glassy phase of SiO_2 – is of particular interest due to its unique mechanical (high strength, low coefficient of thermal expansion), optical (high transparency over a broad spectrum, low dispersion, etc.) and chemical properties (inert to most chemicals) which make it a particularly interesting substrate for micro-devices in which optical, mechanical and fluid-handling function can be combined all together or separately, thanks to the use of femtosecond micromachining [4]. At the micro and nanoscale, amorphous silica exhibits unconventional behaviour such as pseudo-plastic failure and deformation [5-6].

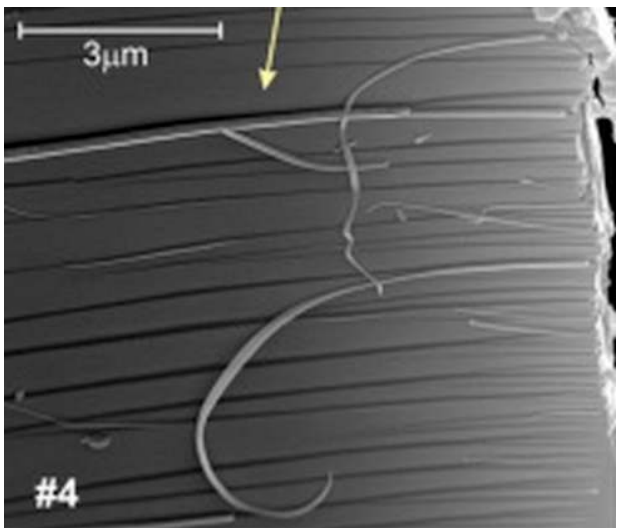

Figure 1. *Bellouard* [7] reported the evidence of localized nano plastic flow via studies of fused silica flexures under high bending stresses.

However, the micromechanical behaviour of fused silica as well as its polymorphic phases remains largely unexplored, due to the inherent experimental difficulties associated with it.

In this work we present a monolithic device, entirely made of fused silica, which is not only able to investigate size effects of fused silica itself, but is also particularly suitable for the mechanical characterization of silica's laser- induced polymorphic structures. The most attractive feature of this device is that it is fabricated and fully operated by the *same* femtosecond laser. This measurement method allows testing materials without mechanically interacting with it and therefore offers the benefit of miniaturization of test specimens, down to nano scale.

In this paper, we firstly present the working principles of the device [8]. Then, we discuss on the underlying physical mechanisms that enable a femtosecond laser to fabricated, operate and characterize a monolithic device with particular emphasis on the use of the third harmonic generation (THG) as a metrology tool. Finally, we demonstrate preliminary results on the stress-stain curve of a used silica beam subjected to tensile stress states as high as 1.8 GPa.

2 Working principles

The physical mechanisms that set the same femtosecond-laser in conjunction with photoelasticity measurements capable of fabricating, actuating and fully characterizing the device are mentioned here:

- Femtosecond laser micromachining is used for the fabrication of the monolithic device.
- *The same* femtosecond laser by inducing controlled variation to the system is used for loading the specimen.
- A flexure-based mechanism is used to amplify the strain of the test beam, turning it to measurable deformation.

[a] Corresponding author: christos.athanasiou@epfl.ch

- *The same* femtosecond laser in another operating regime is used as an in situ characterization tool to measure amplified deformations
- Photoelacticity measurements are used for stress monitoring.

3 Device Operation

3.1 Overview of the device's operation

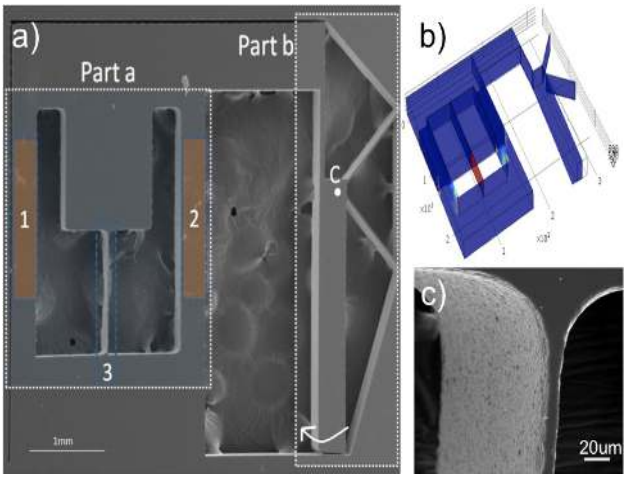

Figure 2. (a) Micro-tensile tester scanning electron microscope image. The overall dimensions of the system are 2.5 mm×2,9 mm. Part a is the loading cell while part b is the displacement amplification sensor. (b) A finite element analysis image for the system loaded is shown. (c) Magnified view of the dog-bone specimen. The rounded corners are designed as such to minimize stress concentrations in the test beam.

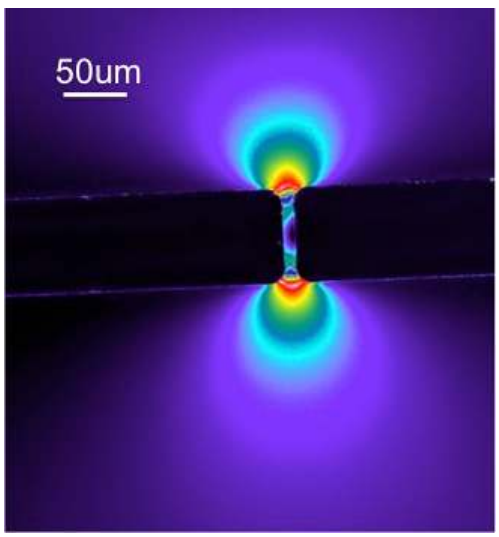

Figure 3. Retardance false colour map of the test beam. The stress is uniformly distributed in the beam. The highest stress is found in the regions close to the attached parts of the beam with the specimen.

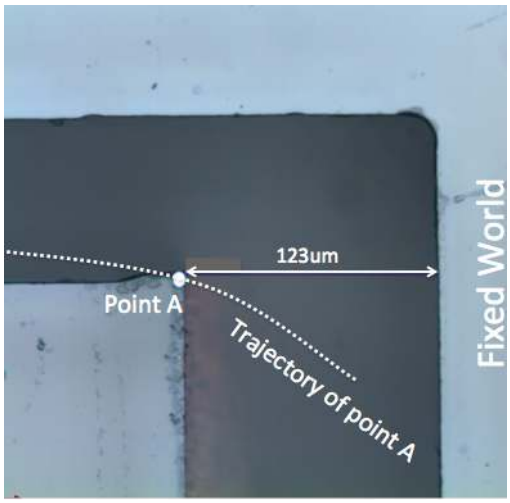

Figure 4. Optical microscopy image of the output of the displacement's amplification sensor. The displacement is measured as the distance of point's A trajectory in respect to a fixed point. This displacement corresponds to the actual strain of the test beam.

The tensile tester consists of two parts (shown in Fig. 2a): the loading cell (part a) and the displacement amplification sensor (part b). The tensile tester is fabricated using a femtosecond laser and chemical etching according a process described later.

To load the microscale beam (thin bar 3 in part a of Fig. 2a), we use the *same* femtosecond laser to re-expose the specimen but only in the zones 1 and 2. Indeed, as demonstrated in [9], laser exposure induces a net volume expansion in the operating regime described above. Here, we take advantage of this effect to generate a net expansion of the two loading bars (bars 1,2 in part a of Fig. 2a). By writing a given number of adjacent planes - each of them consisting of multiple lines writing across the specimen thickness, the applied load can be tuned to virtually any desired level. As an illustration, in the example shown in Fig. 3,4, 1200 planes were written.

The corresponding stress of 1.65 GPa. in the test beam (label 3 in Fig. 2a) is achieved. It is measured with polarized light microscopy (Fig. 3) and is consistent with the stress of 1,51 GPa. calculated using finite method analysis software (COMSOL) (Fig. 2b).

To measure the beam elongation resulting from the stress load, the displacement is mechanically amplified using a flexure-based lever mechanism (part b in Fig. 2a). This mechanism consists of two beams (mounted 45 degrees to the long lever beam) that form a hinge with a remote rotation centre (C indicated in part b of Fig. 2a). This hinge is connected to the main load cell. When a load is applied, the load cell induces a mechanical moment on the hinge that pivots. Using this mechanism, the beam elongation creates a corresponding amplified motion of the elongated beam. By choosing a point of the elongated beam (point A in fig. 4) and measuring its trajectory in respect to a fixed point, we measure the output displacement of the amplification sensor.

3.2 Device preparation and loading principle

3.2.1 Femtosecond laser fabrication

Femtosecond laser machining is used for the fabrication of the flexure-based micro-tensile testing device. This two-step process is described in great detail elsewhere [10].

1/ The first step is to expose the silica substrate to low-energy pulses, below the ablation threshold. During this step, the material structure is locally modified, resulting to an accelerated HF etching rate in the laser exposed regions.

2/ The second step of the process is the chemical etching, where the laser modified-substrate is dipped into a low concentration HF bath (2,5%). Following etching, the part is rinsed in de-ionized water and dried.

3.2.2 Laser-induced volume variation for as a loading tool

Recently, *Champion et al.* [11] reported a method for quantifying localized volume variations in fused silica induced by femtosecond lasers as a function of laser exposure parameters. Interestingly, under certain exposure conditions a volume expansion of 0.03% was measured. Here, we take advantage of this effect to apply incremental load to the test beam. The specimen is re-exposed to the same femtosecond laser that we used for its fabrication but this time to load the test beam.

3.2.3 Laser system

Our experimental setup is limited to the use of a femtosecond laser, positioning stages and a 250um thick silica substrate. The laser emits 270fs- pulses at 1030 nm from a Yb-fiber amplifier operated at 800 kHz. The laser bema is focused using a 20x objective with a numerical aperture (NA) of 0.40. The three linear positioning stages, on which the specimen is mounted, provide three degrees of freedom movement with an accuracy of 800 nm at the operated speeds.

For the fabrication of the device, a scanning speed of 12mm/s with energy per pulse of 250 nJ is used. After the exposure, the device is kept in an HF bath for 24h. The re-exposure of the specimen for the induction of the desired volume variation is implemented by scanning adjacent lines with a writing speed of 10mm/s and energy per pulse of 220 nJ.

In the case of the device fabrication, circular polarization is used.

3.3 Measurement principles

3.3.1 Stain Measurements & Third-harmonic generation (THG) as an in situ edge detection tool

Although spatial displacement measurements in the micro- scale can be performed by various tools i.e. common optical microscopy in conjunction with image analysis, all the available techniques require repositioning of the device from the laser stages, which can eventually turn into a destructive process due to the difficulties of manipulating brittle micron scale samples. To overcome such problems, we use of the same laser as the one that fabricated and operated the microtensile tester but this time at lower energy pulses (50 nJoule per pulse), so as no modification in the material to be made, to accurately measure the output displacements of the test beam.

THG is a surface enhanced phenomenon, due to its dependence on the third order susceptibility ($\chi^{(3)}$) and refractive indices of the materials that form the surface. As demonstrated firstly by *Squier* [12] and later by others [13-14], when using tightly focused high peak power, ultrashort pulses, THG can become a highly operative microscopy tool. Here we take advantage of its use by scanning the femtosecond laser beam across the specimen after its loading. This way, we can estimate the strain of the test beam, not only without mechanically interacting with the specimen, but also without even removing it from the laser platform.

In fig. 5, the THG scanned signal acquired by crossing vertically the surface of a test sample is illustrated.

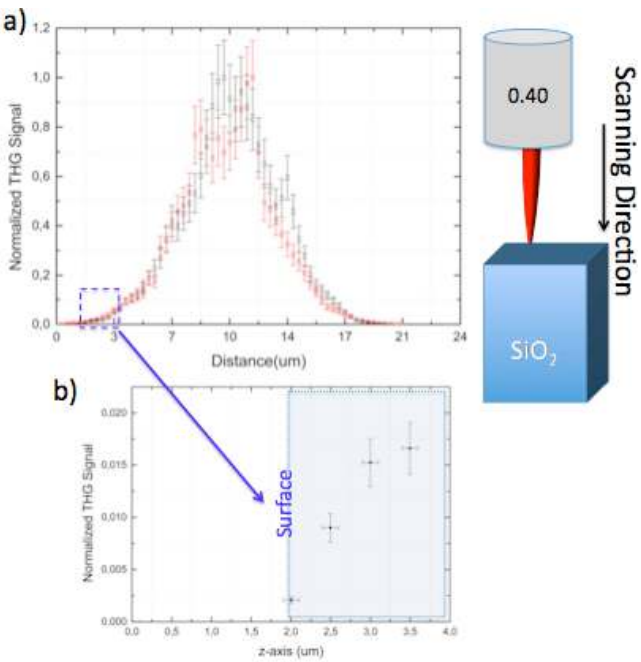

Figure 5. (a) THG scanned signal acquired by crossing vertically the surface of a test sample (b) The sharp transition of the acquired signal helps us define easily the surface of the sample.

There is a sharp transition of the signal at the surface of the material upon the first interaction of the beam spot with the sample (fig 5b). We attribute the plateau (fig. 5a) as the intersection of the ellipsoid's beam waist with the surface of the sample.

In fig. 6, the THG scanned signal acquired across the edge of a test specimen is shown.

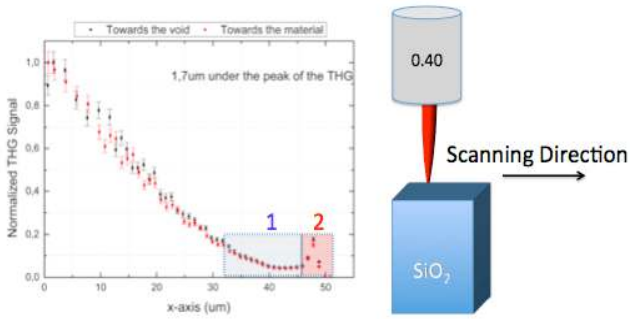

Figure 6. THG scanned signal across the edge of a test sample. In region 1 there is a decay of the signal while region 2 indicates a small spike thanks to which we can perform sub-surface edge detection.

Interestingly, the intensity of the THG signal decays as illustrated in part 1 of fig 6, but eventually rises again as indicated in part 2, forming a small spike. The existence of the spike is attributed to the position where the intersection of the beam with the side surface takes place, while the signal decay at region 1 to total internal reflection. By scanning deeper in the material, we observe that the peak still appears at the same place and eventually disappears only after 13 μm in the depth of the material.

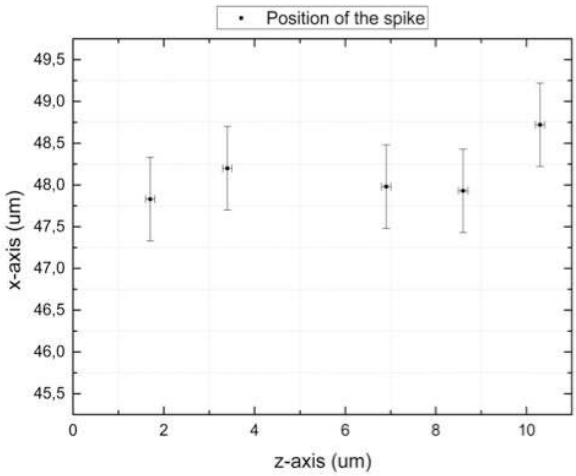

Figure 7. Position of the spike when scanning in different depths of the material. Therefore, there is the capability of the THG to perform subsurface edge-detection.

This measuring technique is capable of detecting subsurface edges -since the position of the spike remains constant (fig. 7), therefore it is a suitable tool for measuring distances even up to 13 μm deep in the material. The measurement accuracy of this technique is estimated to be less than 250 nm.

The THG as a metrology tool does not offer the appealing measurement accuracy achieved by other tools [15-16]. Nevertheless, it offers the advantage of performing *in situ* characterization and therefore dramatically facilitates challenges associated with the manipulation and repositioning of the device.

3.3.2 Stress Measurement

Stress in transparent materials induces birefringence that in turn introduces retardance for the light passing through the specimen [17]. The retardance levels induced in the test beam can be measured using a dedicated microscope (Polscop) and is directly related to the principle stress components according to equation 1.1:

$$\sigma_1 - \sigma_2 = \frac{R}{T(C_1 - C_2)} \qquad (1.1)$$

where C_1-C_2=C is the stress optic coefficient and is equal to $3.55*10^{-12}$ Pa^{-1} for fused silica at 546nm, which is the wavelength that the system operates. The coefficient C is expressed by $C=(n^3/2)(\pi_{11}-\pi_{12})$ where π_{11} and π_{12} are the piezo-optic constants for fused silica [18] and n the refractive index of the material at 546nm. T is the thickness of the sample and R is the measured retardance.

4 Tensile testing: Preliminary results

A small surface of 4 μm^2 in the center of the test beam is used for the estimation of the stress-induced retardance. The stress level is calculated by equation 1.1. The highest level of stress achieved was 1,65 GPa. and the beam failed for a stress level ranging between 1,7 and 1,8 GPa. The specimen's dimensions are (L × W × D) 80 μm × 12 μm × 80 μm. The in-plane dimensions of the test beam were measured the THG, while the thickness was estimated by scanning electron microscopy images.

The strain of the test beam is calculated from the measured displacement of the amplification sensor. A first order model for the response of the sensors used.

As a proof of concept, the elastic modulus of fused silica is estimated (fig. 8) and is consistent with the values referred at the literature (ranging between 72-73 GPa. [19-20]). The measurement deviation is attributed to a combination of the shear stress component and the non-linear displacement of the amplification sensor.

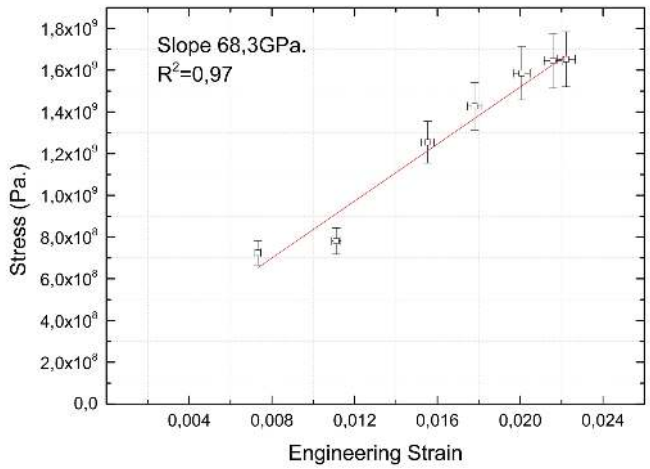

Figure 8. Stress vs. Strain curve of fused silica resulting to the estimate of the elastic modulus using a first oder model of the mechanism.

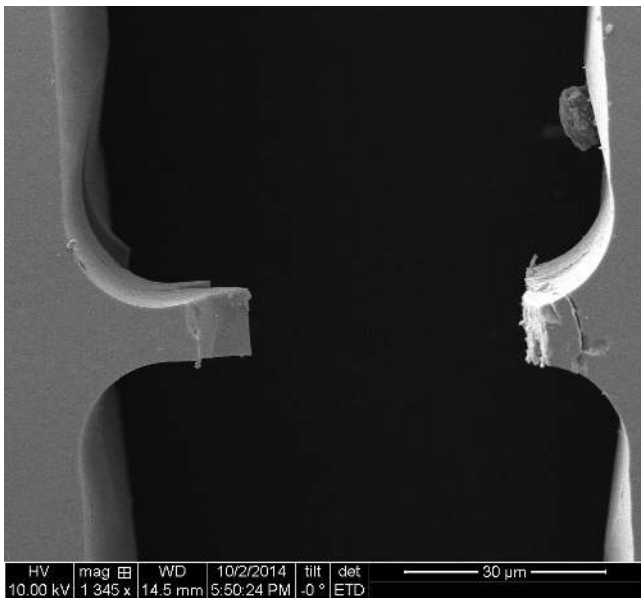

Figure 9. Scanning electron microscopy image of the test beam after its failure. The test beam failed for a stress between 1,7 GPa. and 1,8 GPa.

5 Discussion

A novel and versatile technique to perform microtensile testing of micro specimens of fused silica reaching high stress levels in the order of 1,8GPa. is proposed. The bending stresses are significantly high (10% of the desired uniaxial stress (fig.9) and will be eliminated in future versions of the tensile tester either by optimizing the loading step or by mechanically guiding the loading cell.

In summary, we have demonstrated that *the same* femtosecond laser is capable of fabricating and fully operating a monolithic tensile tester by directly measuring the elastic modulus of silica. This instrument will be further used for the study of silica's laser-induced composite structures at the micro- and nano- scales, whose properties remain largely unexplored.

Acknowledgments

The paper is dedicated to the memory of Giuseppe Melpignano, friend and former colleague of the authors, who passed away the 18th of April 2015.

References

1. S.T. Pantelides, M. Long, Perg. Pr., NY, (1978)
2. D. Bonamy, L. Ponson, S. Prades, E. Bouchaud, C. Guillot. PRL **97**, 13 (2006)
3. R.C. David, T.S. Duffy, E. Ohtani, 1. ed. Amsterdam: Elsevier (2004)
4. Y. Bellouard, JLMN **7**, 1 (2012)
5. E. Bouchaud, C.R.Phys. **15**, 6 (2014)
6. F Célarié, S. Prades, D. Bonamy, L. Ferrero, E. Bouchaud, C. Guillot, C. Marlière. PRL **90**, 7 (2003)
7. Y. Bellouard, OPT **1**, 5 (2011)
8. C.E Athanasiou, B. McMillen, Y. Bellouard. AW1H.6. OSA (2014)
9. A. Champion, Y. Bellouard, OPT, **2**, 6 (2012)
10. Y. Bellouard, A. Said, M. Dugan, P. Bado, Opt E press **12**, 10 (2004)
11. A. Champion, Ph.D. thesis, TU/e (2015)
12. J. Squier, M. Müller, Appl. Opt. **38**, 27 (1999)
13. G.D. Marshall, A. Jesacher, A. Thayil, M. J. Withford, M. Booth, Optics Letters **36**, 5 (2011)
14. R. Tasgal, Y. Band, PRL **70**, 5 (2004)
15. T. Wilhein, B. Kaulich, E. Di Fabrizio, F. Romanato, S. Cabrini, J. Susini, APL **78**,14 (2001)
16. S. Lawman, H. Liang, Appl. Opt. **50**, 32 (2011)
17. L. Fang , Ph.D. thesis, GIT (2010)
18. T.N. Vasudevan, R.S. Krishnan, J. Phys. D. **5**, 12 (1972)
19. S. Spinner, J AM CERAM SOC **39**, 3 (1956)
20. Y. Bellouard, T. Colomb, C. Depeursinge, M. Dugan, A. Said, P. Bado, Opt. Express **14**, (2006)